# Learning Instance and Task-Aware Dynamic Kernels for Few Shot Learning

Rongkai Ma<sup>1</sup> Pengfei Fang<sup>2,3\*</sup> Gil Avraham<sup>1</sup> Yan Zuo<sup>3</sup> Tom Drummond<sup>4</sup> Mehrtash Harandi<sup>1,3</sup>
<sup>1</sup>Monash University, <sup>2</sup>Australian National University, <sup>3</sup>CSIRO, <sup>4</sup>The University of Melbourne

### **Abstract**

Learning and generalizing to novel concepts with few samples (Few-Shot Learning) is still an essential challenge to real-world applications. A principle way of achieving few-shot learning is to realize a model that can rapidly adapt to the context of a given task. Dynamic networks have been shown capable of learning content-adaptive parameters efficiently, making them suitable for few-shot learning. In this paper, we propose to learn the dynamic kernels of a convolution network as a function of the task at hand, enabling faster generalization. To this end, we obtain our dynamic kernels based on the entire task and each sample, and develop a mechanism further conditioning on each individual channel and position independently. This results in dynamic kernels that simultaneously attend to the global information whilst also considering minuscule details available. We empirically show that our model improves performance on few-shot classification and detection tasks, achieving a tangible improvement over several baseline models. This includes state-of-the-art results on 4 few-shot classification benchmarks: mini-ImageNet, tiered-ImageNet, CUB and FC100 and competitive results on a few-shot detection dataset: MS COCO-PASCAL-VOC.

### 1. Introduction

Despite the great success of the modern deep neural networks (DNNs), in many cases, the problem of adapting a DNN with only a handful of labeled data is still challenging. Few-Shot Learning (FSL) aims to address the inefficiencies of modern machine learning frameworks by adapting models trained on large databases for novel tasks with limited data [13, 32, 45, 59].

Early approaches of FSL learned a fixed embedding function to encode samples into a latent space, where they could be categorized by their semantic relationships [44,45,59]. However, such fixed approaches do not account for category differences [36], which may exist between already learned tasks and novel tasks. Ignoring these discrepancies

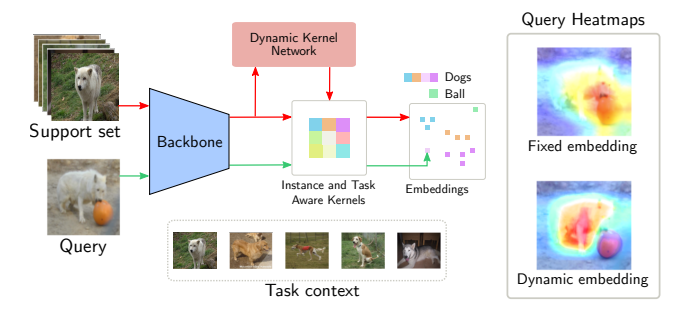


Figure 1. Typical FSL models learn fixed embeddings, which are not flexible enough to rapidly adapt to novel tasks. Our method instead uses a dynamic kernel network to produce a set of dynamic parameters which are both instance and task-aware.

can severely limit the adaptability of a model as well as its ability to scale in the FSL setting. Although methods that adapt embeddings [31,49,58] attempt to address this issue, they still utilize fixed models which lack full adaptability and are constrained to previously learned tasks. Another group of approaches, such as [13, 32], adapt models with a few optimization steps. Given the complexity of the loss landscape of a DNN, such methods come short compared to metric-based solutions [53].

Dynamic kernel approaches have been shown to be computationally efficient [61] relative to optimization-based solutions, resulting in the models capable of encoding the novel information at the parameter level [20]. A very recent study [55] showed that dynamic kernel methods are effective when applied to FSL via the learning of input-conditioned filters, enabling the realization of adaptive models; a key limitation of this dynamic kernel method is that only the per-class level information is utilized via class prototypes.

Arguably, when learning new tasks with sparse data, it is vital to fully utilize information on both an instance and task-level for efficiency. As an example, when given the task of differentiating between dog breeds (Fig. 1), both task and instance-level information is required; it is important that we are sensitive enough to distinguish the minuscule details between different dog breeds (instance-level), yet can still focus on the global knowledge required to filter

<sup>\*</sup>Corresponding author.

out irrelevant, non-task related objects (task-level).

In this paper, we propose a novel, dynamic approach for FSL tasks. Our method is realized by a dynamic kernel that can encode both instance-level and task-level features via jointly learning a dynamic kernel generator and a context learning module. The dynamic kernel generator adaptively produces an instance kernel by exploiting the information along the spatial and channel dimensions of a feature map in a decoupled manner. It further incorporates information from the frequency domain resulting in a rich set of descriptive representations. The context learning module refines the support features into a task-specific representation which is used to produce the task-specific kernel. The resulting instance and task-specific kernels are fused to obtain a dynamic kernel which is INStance and Task-Aware (INSTA). Our method differentiates from approaches such as FEAT [58] and GLoFa [31] by learning a set of dynamic parameters adaptive to the novel tasks instead of employing fixed models during inference. Furthermore, in contrast to optimization-based methods [13], our approach can adapt the model parameters without the requirements of backpropagation during the inference stage. We offer the following contributions:

- We propose a novel FSL approach to extract both instance and task-specific information using dynamic kernels.
- We offer the first FSL framework capable of being evaluated on both classification *and* detection tasks.
- Empirically, we offer substantial improvements over several FSL baselines, including optimization-based and metric-based approaches.

### 2. Related Work

The family of few-shot learning literature is broad and diverse. However, those related to this work are mainly the family of optimization-based methods [3, 13–15, 24, 32, 38, 43] and metric-based methods [4, 11, 42, 44, 45, 49, 58, 59]. **Optimization based methods.** Optimization-based methods such as MAML [13] or Reptile [32] focus on learning a set of initial model parameters that can generalize to new tasks (or environments) with a small number of optimization steps and samples without severe over-fitting. Furthermore, in most cases, this group of methods present a framework trained with a bi-level optimization setting [15], which provides a feasible solution to adapt the model to the test set from the initialized model.

Our proposed framework is similar to the optimizationbased methods [1, 2, 6, 25, 30] in the sense that the model parameters are task-adaptive. However, our solution does not require backpropagation during inference to achieve so. Furthermore, our method can be incorporated with optimization-based methods, and empirically we observed that such construction yields performance improvement. This will be demonstrated in § 4.

Metric-based methods. In few-shot learning literature, the metric-based methods aim to define a metric to measure the dis/similarity between samples from a few observations [8,22,28,29,39,54,56,60]. ProtoNet [44] achieves this by learning a fixed latent space where the class representations (i.e., prototype), obtained by averaging the features from the same class, are distinctive for different classes. DeepEMD [59] formulates the query-support matching as an optimal transport problem and adopts Earth Mover's distance as the metric. One commonality in the aforementioned methods is the fact that all employ a fixed embedding space when facing novel tasks, which essentially limits their adaptability. On the other hand, many previous methods suggested to adapt the embeddings to the novel tasks [12, 17, 31, 33, 41, 47, 58]. CTM [26] proposes to produce a mask to disregard the uninformative features from the support and query embeddings during inference. MatchingNet [49] uses a memory module to perform sample-wise embedding adaptation and determines the query label by a cosine distance. TADAM [33] proposes to learn a dynamic feature extractor by applying a linear transformation to the embeddings to learn a set of scale and shift parameters. FEAT [58] and GLoFa [31] provide an inspiring way to perform the embedding adaptation using a set function.

Our contribution is complementary to the aforementioned methods. We aim to learn a set of dynamic kernels via exploiting the instance and task-level information according to the task at hand. This results in a more distinctive and descriptive representation, which effectively boosts the performance of these methods directly relying on constructing a metric space.

**Dynamic kernels.** The application of dynamic kernels solutions within the domain of Few-shot learning is less explored in the current literature. However, it has been demonstrated useful when labels are abundant [5,7,16,19,46,48,51,61]. Zhou *et al.* [61] have proposed to use decoupled attention over the channel and spatial dimensions. This results in a content-adaptive and efficient method that provides a feasible way to achieve task-adaptive FSL.

To leverage the effectiveness of the dynamic kernel into few-shot learning tasks, [55] propose to learn dynamic filters for the spatial and channels separately via grouping strategy. The resulted kernels are then applied to the query to produce a support-aligned feature. Due to the usage of grouping, the performance might sacrifice for efficiency [61]. Inspired by these methods, our INSTA produces dynamic kernels that are both instance-aware and task (or episodic)-aware while also incorporating valuable frequency patterns; as such, our method produces more informative and representative features.

### 3. Method

In this section, we introduce our proposed INSTA. Note that while we present our method in terms of few-shot classification, the proposed approach is generic and can be used to address other few-shot problems, including structured-prediction tasks such as few-shot object detection (see § 4.3 for details).

#### 3.1. Problem Formulation

In what follows, we will give a brief description of the problem formulation for few-shot classification. The vectors and matrices (or high-dimensional tensors) are denoted by bold lower-case letters  $(e.g., \mathbf{X})$  and bold upper-case letters  $(e.g., \mathbf{X})$  throughout this paper. The FSL aims to generalize the knowledge acquired by a model from a set of examples  $\mathcal{D}_{train} = \{(\mathbf{X}_i, y_i) | y_i \in \mathcal{C}_{train}\}$ , to novel and unseen tasks  $\mathcal{D}_{test} = \{(\mathbf{X}_i, y_i) | y_i \in \mathcal{C}_{test}\}, \mathcal{C}_{train} \cap \mathcal{C}_{test} = \emptyset$ , in a low data regime.

We follow the meta-learning protocol to formulate FSL with episodic training and testing. Specifically, an episode  $\mathcal{E}$  consists of a support set  $\mathcal{X}^s = \{(\boldsymbol{X}_{ij}^s, y_i^s) | i = 1, \ldots, N, j = 1, \ldots, K, y_i^s \in \mathcal{C}_{train}\}$ , where  $\boldsymbol{X}_{ij}^s$  denotes the j-th sample in the class  $y_i^s$  and the query set  $\mathcal{X}^q = \{(\boldsymbol{X}_i^q, y_i^q) | i = 1, \ldots, N\}$ , where  $\boldsymbol{X}_i^q$  denotes a query example 1 sampled from class  $y_i^q$  (the test setup is the same as training but the episodes are sampled from  $\mathcal{D}_{test}$ ). Such a formulation is known as N-way K-shot, where the goal is to utilize the support samples and their labels to obtain  $\Theta^*$ , the optimal parameters of the model, such that each query is classified correctly into one of the support classes. The object of network training follows that:

$$\Theta^* = \arg\min_{\boldsymbol{X}_i^q \in \mathcal{X}^q} \mathcal{L}(f_{\boldsymbol{\Theta}}(\boldsymbol{X}_i^q | \mathcal{X}^s), y_i^q), \qquad (1)$$

where  $f_{\Theta}$  represents the entire model parameterized by  $\Theta$ .

### 3.2. Model Overview

We first provide an overview of our model (see the sketch of the pipeline in Fig. 2). Overall, our framework is composed of three modules, the backbone network  $f_{\theta}$ , the dynamic kernel generator  $f_{\omega}$ , and the context learning module  $f_{\phi}$ . The backbone network first extracts the feature maps from the input images, followed by a two-branch dynamic kernel network to obtain our proposed dynamic kernels. Specifically, the dynamic kernel generator independently refines the features in the support set to produce the instance kernel (i.e.,  $G^{in}$ ) in one branch. In another branch, the context learning module  $f_{\phi}$  first produces a task-specific representation by refining and summarizing the features from

the entire support set, which is then used as the input of the dynamic kernel generator to produce the task-specific kernel (i.e.,  $G^{ta}$ ) adaptively. The dynamic kernel generator is shared across these two branches to generate the instance kernel and the task-specific kernel. Such a two-branch design enables the network to be aware of both the instancelevel feature and global context feature of the support set. The design choice is justified in § 4. Finally, both the instance and task-specific kernels are combined and employed to boost the discrimination of instance features in the support set. The task-specific kernel is applied to the query feature maps for refining the representation without extracting a query instance kernel. Given the adapted support and query features, any post-matching algorithm (e.g., metricbased or optimization-based FSL) can be employed seamlessly to achieve the few-shot classification task.

### 3.3. Dynamic Kernel Network

In this part, we provide a detailed description of the twobranch network to obtain our dynamic kernels. We first introduce the branch of the instance kernel followed by that of the task-specific kernel. In the end, we discuss the usage of our dynamic kernels on support and query feature maps.

#### 3.3.1 Instance Kernel

The central component of the instance kernel branch is the dynamic kernel generator, which receives the support feature map as input and produces the instance kernel adaptively. An essential problem one may face is that the feature map extracted by modern DNNs usually has a large size (e.g.,  $640 \times 5 \times 5$  for ResNet-12). As such, we need to identify  $c_{out} \times c \times k \times k$  amount of parameters for the dynamic kernel, where the  $c_{out}$  is the output channel size (we consider  $c = c_{out}$  in our paper), c is the input channel size, and k is the kernel size. This poses a significant issue since the generated dynamic kernel is prone to overfitting given the limited data of FSL. To tackle this problem, we consider designing our dynamic kernel generator in a decomposed manner [61]. As such, we develop a channel kernel network and a spatial kernel network to produce a kernel for each channel and each spatial location independently. This design exploits the information per data-sample to a large extent while reducing the number of parameters of a dynamic kernel, which greatly fits the low data regime of FSL. Fig. 3 illustrates the pipeline of the proposed dynamic kernel generator. In what follows, we detail out the operations of the channel and spatial kernel networks.

Channel Kernel Network. Given the support set images  $\mathcal{X}^s = \{\boldsymbol{X}_{11}^s, \dots, \boldsymbol{X}_{NK}^s | \boldsymbol{X}_{ij}^s \in \mathbb{R}^{C \times H \times W}\}$ , where C, H, and W indicate the channel, height, and width of an image, respectively, the backbone network first extracts a feature map from each image, as  $\mathcal{S} = f_{\theta}(\mathcal{X}^s)$ , with  $\mathcal{S} = \{\boldsymbol{S}_{11}, \dots, \boldsymbol{S}_{NK} | \boldsymbol{S}_{ij} \in \mathbb{R}^{c \times h \times w}\}$ . The feature map for the query sample can be obtained in a similar fashion,

<sup>&</sup>lt;sup>1</sup>Without losing generality, we use one sample per class as a query for presenting our method. In practice, each episode contains multiple samples per query class.

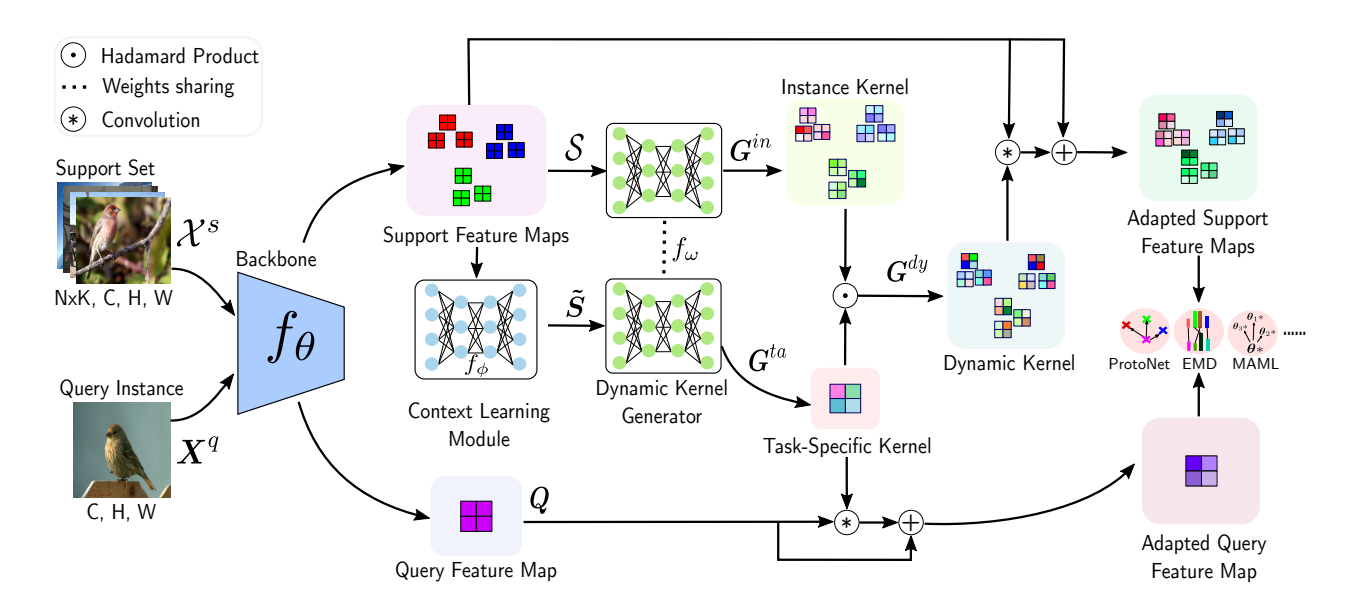


Figure 2. The framework of our method. Given the support set  $\mathcal{X}^s$  and the query sample  $X^q$ , the backbone network  $f_\theta$  first encodes them into a representation space as  $\mathcal{S} = \{S_{11}, \dots, S_{NK}\}$  and Q. Then a dynamic generator  $f_\omega$  is used to produce an instance kernel for each support sample. Meanwhile, a context learning module  $f_\phi$  is used to refine and aggregate the context of the entire support feature maps to produce a task-specific representation, which is then used as the input of  $f_\omega$  to obtain the task-specific kernel. Note the instance kernel and task-specific kernel share the parameters across  $f_\omega$ . Finally, a dynamic kernel that is both instance-aware and task-aware is applied to the support feature maps, while the task-specific kernel is applied to the query feature map to obtain the adapted representations.

as  $Q_i = f_{\theta}(X_i^q)$ . Once we have the feature map  $S_{ij}$ , a common practice to realize the channel kernel network follows the SE block [18], as done for example in [7]. In the SE block, global average pooling (GAP) is performed over the feature map to encode the global representation, which is fed to the following sub-network for channel-wise scaling. The drawback of this design is that the GAP operator mainly preserves the low frequency components of the feature map, as shown in [34] (averaging is equivalent to low-pass filtering in the frequency domain). Thus, GAP discards important signal patterns in the feature map to a great degree. Clearly, low-frequency components cannot fully characterize the information encoded in a feature map, especially in the low data regime. We will empirically show this in § 4.4.

To mitigate this issue, we opt for multi-spectral attention (MSA) to make better use of high-frequency patterns in the feature map. Given a feature map  $S^2$ , we equally split the feature map into n smaller tensors along the channel dimension (in our experiments n=16), as  $\{S^0, S^1, \ldots, S^{n-1} | S^i \in \mathbb{R}^{\frac{c}{n} \times h \times w}\}$ . Then, each channel of the tensor  $S^i$  is processed by a basis function of a 2D-Discrete Cosine Transform (DCT) following the work of Qin *et al.* [34]. As a result, we obtain a real-valued feature vector in the frequency domain as  $\tau^i = \mathrm{DCT}(S^i), \tau^i \in$ 

 $\mathbb{R}^{c/n}$ , which is the frequency-encoded vector corresponding to  $S^i$ . The frequency-encode vector for S is obtained by concatenating  $\tau^i$ s as:

$$\tau = \operatorname{concat}(\tau^0, \tau^1, \dots, \tau^{n-1}),$$
 (2)

where  $\tau \in \mathbb{R}^c$ . Please refer to the supplementary material for the theoretical aspects of the MSA module. As compared to the global feature obtained by GAP, frequency-encoded feature  $\tau$  contains more diverse information patterns, which brings extra discriminative power to our model. This will be empirically discussed in § 4.4.

Once we obtain  $\tau$ , a light-weight network is used to produce the channel kernel values adaptively. This network is realized by a two-layer MLP (or  $1 \times 1$  convolution), with architecture as  $c \to \sigma \times c \to \text{ReLu} \to k^2 \times c$ , where  $0 < \sigma < 1$ , and k controls the size of receptive field in the dynamic kernel (practically, we set  $\sigma = 0.2$  and k = 3). Then we reshape the output vector into a  $c \times k \times k$ -sized tensor, denoted by  $\mathbf{G}^{ch}$ . We can obtain the final channel dynamic kernel  $\hat{\mathbf{G}}^{ch} \in \mathbb{R}^{c \times h \times w \times k \times k}$  via applying batch normalization (BN) and spatial-wise broadcast to  $\mathbf{G}^{ch}$ .

**Spatial Kernel Network.** Independent to the channel kernel network, our spatial kernel network adaptively produces a convolution kernel  $G_{a,b}^{sp} \in \mathbb{R}^{k \times k}$  for each spatial location of a feature map  $(i.e., S_{:,a,b})$ . This is achieved by using a  $1 \times 1$  convolution layer, with the architecture of  $(c, k^2, 1, 1)$  and the reshape operation. Therefore, the spatial kernel  $G^{sp}$ 

 $<sup>^2{\</sup>rm The}$  subscripts have been omitted to avoid cluttering of notations. Here,  ${\bm S}$  denotes any feature map in the support set.

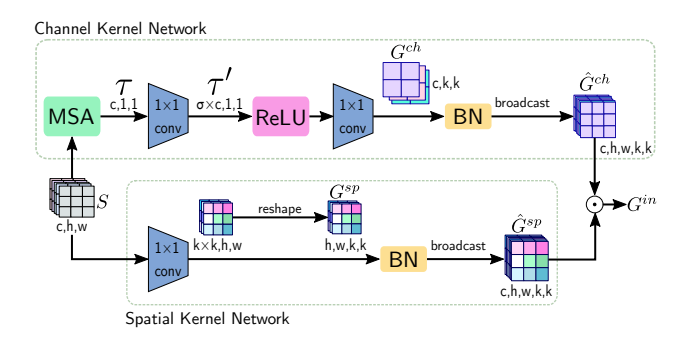


Figure 3. The architecture of dynamic kernel generator. We adopt a decomposed architecture to produce dynamic kernels for the channels and spatial dimensions independently. This results in a light-weight kernel, which greatly fits the low-data regime of FSL.

for all the spatial locations of a feature map S has a size of  $h \times w \times k \times k$ . We then obtain the final spatial dynamic kernel  $\hat{G}^{sp} \in \mathbb{R}^{c \times h \times w \times k \times k}$  by applying the BN and channel-wise broadcast to  $G^{sp}$ .

Finally, to unify the channel and spatial dynamic kernels, we apply the Hadamard product between the  $\hat{G}^{ch}$  and  $\hat{G}^{sp}$  to obtain the final instance dynamic kernel  $G^{in}$  for each support instance as:

$$\mathbf{G}^{in} = \hat{\mathbf{G}}^{sp} \odot \hat{\mathbf{G}}^{ch},\tag{3}$$

where  $G^{in} \in \mathbb{R}^{c \times h \times w \times k \times k}$ . Notably, the number of parameters of our dynamic kernel is much less than a normal convolution kernel ( $c \times h \times w \times k^2 \ll c_{out} \times c \times k^2$  given  $c_{out} = c = 640$  and h = w = 5).

### 3.3.2 Task-Specific Kernel.

Adapting according to the whole context of support set is essential for FSL since it contains essential information of the task [33]. Following this intuition, we propose to use a context learning module  $f_{\phi}$  to produce a fully context-aware representation for the support set by refining and aggregating the intermediate features. To be specific, we use four  $1 \times 1$  convolution layers with a summation layer in the middle of the network (see Fig. 4). Formally, this task representation can be obtained by:

$$\tilde{\mathbf{S}} = f_{\phi}(\mathcal{S}),\tag{4}$$

where  $\tilde{S} \in \mathbb{R}^{c \times h \times w}$  and the  $\mathcal{S}$  denotes the entire support set. Then this task representation  $\tilde{S}$  is used as the input to the dynamic kernel generator (see § 3.3.1), following the same process of obtaining the instance dynamic kernel  $G^{in}$  to adaptively produce our task-specific kernel  $G^{ta} \in \mathbb{R}^{c \times h \times w \times k \times k}$ .

### 3.3.3 Dynamic Kernel

Once we have the instance and task-specific kernels, we fuse each instance kernel  $G_{ij}^{in}$  (It refers to the instance kernel of the j-th sample of class i of the support set) with

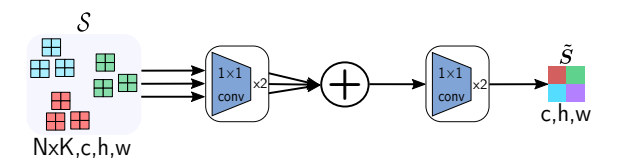


Figure 4. The structure of context learning module. Our context learning module  $f_{\phi}$  receives the entire support feature maps  $\mathcal{S}$  as a bag and aggregates the  $N \times K$  samples in the intermediate layer. Finally, it generates a task-specific representation  $\tilde{\mathbf{S}}$  for the entire support set with a size of  $c \times h \times w$ .

task-specific kernel  $G^{ta}$  using the Hadamard product, such that each dynamic kernel considers both the instance-level and task-level features. Formally, it can be described as:

$$\boldsymbol{G}_{ij}^{dy} = \boldsymbol{G}_{ij}^{in} \odot \boldsymbol{G}^{ta}, \tag{5}$$

where  $G_{ij}^{dy}$  is the final dynamic kernel corresponding to the ij-th sample.

After  $G_{ij}^{dy}$  is obtained, we apply the fused dynamic kernel on its corresponding support feature map  $S_{ij}$  to extract the features. While, we only apply the task-specific kernel  $G^{ta}$  on the query feature map  $Q_i$  since we only know that the query belongs to the task without the label.

This process can be implemented using the Hadamard product between the unfolded feature map and the dynamic kernel. In doing so, the unfold operation first samples a  $k\times k$  spatial region of the input feature map at each time and then stores the sampled region into extended dimensions, thereby obtaining an unfolded support feature map  $S^u_{ij}\in\mathbb{R}^{c\times h\times w\times k\times k}$  and an unfolded query feature map  $Q^u_i\in\mathbb{R}^{c\times h\times w\times k\times k}$ . Then the adapted support and query feature maps are obtained as:

$$\dot{\mathbf{S}}_{ij} = \text{AvgPool2d}(\mathbf{S}_{ij}^u \odot \mathbf{G}_{ij}^{dy}) + \mathbf{S}_{ij}, 
\dot{\mathbf{Q}}_i = \text{AvgPool2d}(\mathbf{Q}_i^u \odot \mathbf{G}^{ta}) + \mathbf{Q}_i,$$
(6)

where  $\dot{S}_{ij} \in \mathbb{R}^{c \times h \times w}$  and  $\dot{Q}_i \in \mathbb{R}^{c \times h \times w}$ . Note that the convolution operation between the dynamic kernel and the feature map in Fig. 2 is equivalent to the average of the Hadamard product between the unfolded feature map and the dynamic kernel over the  $k \times k$  dimension. In our design, we adopt a residual connection between the original and the updated feature maps to obtain the final adapted features. Having the adapted support and query feature maps, any post-matching algorithms can be adopted to achieve FSL tasks. In § 4, we demonstrate that our algorithm can further boost the performance on various few-shot classification models (e.g., MAML [13], ProtoNet [44] and EMD [59]) and the few-shot detection model [10].

# 4. Experiments

In this section, we first evaluate our method across four standard few-shot classification benchmarks: *mini*-ImageNet [35], *tiered*-ImageNet [36], CUB [50], and FC100 [33]. Full details of the implementation are provided in the supplementary material. Furthermore, we evaluate the effectiveness of our framework for the few-shot detection task on the MS COCO and PASCAL VOC datasets [10]. Finally, we provide an ablation study to discuss the effect of each module in our framework. In the following, we will give a brief introduction to each dataset.

#### 4.1. Datasets

*mini*-ImageNet. The *mini*-ImageNet is sampled from ImageNet [9]. This dataset has 100 classes, with each having 600 samples. We follow the standard protocol [35] to split the dataset into 64 training, 16 validation, and 20 testing classes.

*tiered*-ImageNet. Similar to *mini*-ImageNet, *tiered*-ImageNet is also a subset of the ImageNet. This dataset consists of 608 classes from 34 categories and is split into 351 classes from 20 categories for training, 97 classes from 6 categories for validation, and 160 classes from 8 categories for testing.

**CUB.** The CUB is a fine-grained dataset, which consists of 11,788 images from 200 different breeds of birds. We follow the standard settings [27], in which the dataset is split into 100/50/50 breeds for training, validation, and testing, respectively.

**FC100.** FC100 dataset is a variant of the standard CI-FAR100 dataset [23], which contains images from 100 classes, with each class containing 600 samples. We follow the standard setting [33], where the dataset is split into 60/20/20 classes for training, validation and testing, respectively

MS COCO and PASCAL VOC Datasets. In the few-shot detection task, we follow the protocol used in [10] to construct the dataset, where images from 60 categories of the MS COCO dataset are used for training and images from the rest of 20 common categories between MS COCO and PASCAL VOC datasets are used for testing.

### 4.2. Few-Shot Classification

We conduct few-shot classification experiments on three different state-of-the-art models, including MAML [13], ProtoNet [44] and DeepEMD [59] as baselines, and employ the proposed INSTA on top of them. We use the ResNet-10 backbone for the MAML and the ResNet-12 backbone for the other two baselines across all four benchmarks. (Additional ResNet-18 backbone is employed for the ProtoNet experiments on CUB). For a fair comparison, we implement all the baseline models to report the results indicated by

"\*" across Table 1 – Table 4. Notably, for DeepEMD experiments, we adopt the *open-cv* solver instead of the *qpth* solver originally used in the paper to train the network due to resource capacity, which is indicated by "\*."

Moreover, following the the same evaluation protocols in our baseline frameworks [6, 59], we report the mean accuracy with 95% confidence interval (Please refer to supplementary material for more implementation details). mini-ImageNet. As shown in Table 1, our method improves the performance of all the baseline models by a noticeable margin. It is worthwhile to mention that our INSTA can boost the performance of the baseline model ProtoNet by 4.72% and 3.67%, and achieves 67.01% and 83.13% for 5-way 1-shot and 5-way 5-shot settings, which outperforms many recent published models. Furthermore, we can show an improvement over a strong baseline model, i.e. DeepEMD, and achieve state-of-the-art performance on this dataset. We provide more comparison between our approach and other state-of-the-art methods in our supplementary material for mini-ImageNet and tiered-ImageNet.

Model	Backbone	5-way 1-shot	5-way 5-shot
MetaOptNet [24]	ResNet-12	$62.64 \pm 0.61$	$78.63 \pm 0.46$
TADAM [33]	ResNet-12	$58.50 \pm 0.30$	$76.70 \pm 0.30$
FEAT [58]	ResNet-12	$66.78 \pm 0.20$	$82.05 \pm 0.14$
CAN [17]	ResNet-12	$63.85 \pm 0.48$	$79.44 \pm 0.34$
FRN [54]	ResNet-12	$66.45 \pm 0.19$	$82.83 \pm 0.13$
InfoPatch [28]	ResNet-12	$67.67 \pm 0.45$	$82.44 \pm 0.31$
GLoFA [31]	ResNet-12	$66.12 \pm 0.42$	$81.37 \pm 0.33$
DMF [55]	ResNet-12	$67.76 \pm 0.46$	$82.71 \pm 0.31$
MAML* [13]	ResNet-10	$54.73 \pm 0.87$	$66.72 \pm 0.81$
INSTA-MAML*	ResNet-10	$56.41 \pm 0.87$	$71.56 \pm 0.75$
ProtoNet* [44]	ResNet-12	$62.29 \pm 0.33$	$79.46 \pm 0.48$
INSTA-ProtoNet*	ResNet-12	$67.01 \pm 0.30$	$83.13 \pm 0.56$
DeepEMD*♣ [59]	ResNet-12	$67.37 \pm 0.45$	$83.17 \pm 0.75$
INSTA-DeepEMD*♣	ResNet-12	$68.46 \pm 0.48$	$84.21 \pm 0.82$

Table 1. Few-shot classification accuracy and 95% confidence interval on *mini*-ImageNet with ResNet backbones.

tiered-ImageNet. As shown in Table 2, our model consistently brings the performance gain over baseline models. Among baseline models, our model shows a greater performance improvement over MAML than ProtoNet and DeepEMD. Notably, a significant improvement on 5-way 5-shot can be seen over DeepEMD. We attribute this improvement to our model's context module leveraging the categorical nature of this dataset. The results also show that the DeepEMD exhibits a performance gain with our design and outperforms many other recent models, which achieves the state-of-the-art result on this dataset.

**CUB.** The result on the CUB dataset is shown in Table 3, where the performance of all the three baseline models is improved by integrating the proposed INSTA. For the ProtoNet baseline with ResNet-12 backbone, as an example, 4.29% and 3.72% improvements can be observed for 5-way 1-shot and 5-way 5-shot, respectively. Moreover, among

Model	Backbone	5-way 1-shot	5-way 5-shot
MetaOptNet [24]	ResNet-12	$68.23 \pm 0.23$	$84.03 \pm 0.56$
FEAT [58]	ResNet-12	$70.80 \pm 0.23$	$84.79 \pm 0.16$
CAN [17]	ResNet-12	$69.89 \pm 0.51$	$84.23 \pm 0.37$
FRN [54]	ResNet-12	$72.06 \pm 0.22$	$86.89 \pm 0.14$
GLoFA [31]	ResNet-12	$69.75 \pm 0.33$	$83.58 \pm 0.42$
DMF [55]	ResNet-12	$71.89 \pm 0.52$	$85.96 \pm 0.35$
MAML* [13]	ResNet-10	$59.85 \pm 0.97$	$73.20 \pm 0.81$
INSTA-MAML*	ResNet-10	$63.34 \pm 0.92$	$78.01 \pm 0.71$
ProtoNet* [44]	ResNet-12	$68.25 \pm 0.23$	$84.01 \pm 0.56$
INSTA-ProtoNet*	ResNet-12	$70.65 \pm 0.33$	$85.76 \pm 0.59$
DeepEMD*♣ [59]	ResNet-12	$73.19 \pm 0.32$	$86.79 \pm 0.61$
INSTA-DeepEMD*♣	ResNet-12	$73.87 \pm 0.31$	$88.02 \pm 0.61$

Table 2. Few-shot classification accuracy and 95% confidence interval on *tiered*-ImageNet with ResNet backbones.

the improved models, our INSTA-DeepEMD achieves the state-of-the-art results, which are 75.26% and 88.12% for 5-way 1-shot and 5-way 5-shot settings, respectively. Interestingly, with the ResNet-18 backbone, ProtoNet outperforms many state-of-the-art models, and our INSTA can further improve the performance by 2.12% and 2.15% for 1-shot and 5-shot settings, respectively, which further shows the superiority of our method for fine-grained tasks.

Model	Backbone	5-way 1-shot	5-way 5-shot
RelationNet [45]	ResNet-18	$67.59 \pm 1.02$	$82.75 \pm 0.58$
Chen et al. [6]	ResNet-18	67.02	83.58
SimpleShot [52]	ResNet-18	70.28	86.37
Neg-Margin [27]	ResNet-18	$72.66 \pm 0.85$	$89.40 \pm 0.43$
P-transfer [40]	ResNet-12	$73.88 \pm 0.87$	$87.81 \pm 0.48$
MAML* [13]	ResNet-10	$70.46 \pm 0.97$	$80.15 \pm 0.73$
INSTA-MAML*	ResNet-10	$73.08 \pm 0.97$	$84.26 \pm 0.66$
ProtoNet* [44]	ResNet-12	$64.76 \pm 0.33$	$77.99 \pm 0.68$
INSTA-ProtoNet*	ResNet-12	$69.05 \pm 0.32$	$81.71 \pm 0.63$
DeepEMD*♣ [59]	ResNet-12	$74.55 \pm 0.30$	$87.55 \pm 0.54$
INSTA-DeepEMD*♣	ResNet-12	$75.26 \pm 0.31$	$88.12 \pm 0.54$
ProtoNet*	ResNet-18	$75.06 \pm 0.30$	$87.39 \pm 0.48$
INSTA-ProtoNet*	ResNet-18	$77.18 \pm 0.29$	$89.54 \pm 0.44$

Table 3. Few-shot classification accuracy and 95% confidence interval on CUB with ResNet backbones.

FC100. Consistent with the observation in the other benchmarks, the results in Table 4 again show that a performance improvement can be achieved on FC100. Furthermore, both INSTA-ProtoNet and INSTA-DeepEMD achieve comparable performance with the recent state-of-the-art models on FC100, which vividly shows the effectiveness of our approach.

#### 4.3. Few-Shot Detection

**Problem Definition.** Given a query and several support images (each support image only contains one object), a few-shot detection task is to output labels and corresponding bounding boxes for all objects in the query image that belong to support categories. Specifically, few-shot detec-

Model	Backbone	5-way 1-shot	5-way 5-shot
TADAM [33]	ResNet-12	$40.10 \pm 0.40$	$56.10 \pm 0.40$
ConstellationNet [56]	ResNet-12	$43.80 \pm 0.20$	$59.70 \pm 0.20$
MAML* [13]	ResNet-10	$34.50 \pm 0.69$	$47.31 \pm 0.68$
INSTA-MAML*	ResNet-10	$38.02 \pm 0.70$	$51.20 \pm 0.68$
ProtoNet* [44]	ResNet-12	$41.54 \pm 0.76$	$57.08 \pm 0.76$
INSTA-ProtoNet*	ResNet-12	$44.12 \pm 0.26$	$62.04 \pm 0.75$
DeepEMD*♣ [59]	ResNet-12	$45.12 \pm 0.26$	$61.46 \pm 0.70$
INSTA-DeepEMD*♣	ResNet-12	$45.42 \pm 0.26$	$62.37 \pm 0.68$

Table 4. Few-shot classification accuracy and 95 % confidence interval on FC100 with ResNet backbone.

tion follows the N-way K-shot setting, where the support set contains N categories, with each category having K samples. In the following, we will discuss the experiment setup of this task. The implementation details on incorporating our INSTA with the baseline model proposed by Fan *et al.* [10] are included in the supplementary material.

**Experiment Setup.** In this experiment, we follow the training and testing settings in [10], where a 2-way 9-shot contrastive training strategy is adopted, and a 20-way 10-shot setting is used for final testing.

**Results.** We compare our model against the baseline model and other relevant state-of-the-art few-shot detection models. As shown in Table 5, by incorporating the proposed INSTA on the baseline model, improved performance can be seen across all of the metrics. Specifically, as compared to the baseline model, the AP<sub>50</sub> is improved by 3.2% and achieves 23.6%, which empirically shows that our dynamic kernels indeed extract more informative and representative features. Moreover, the proposed INSTA improves the performance of detection for objects of all the scales (refer to AP<sub>s</sub>, AP<sub>m</sub>, and AP<sub>l</sub>), which again illustrates the importance of our context module when adapting to different object scales in a given task.

Model	AP	AP <sub>50</sub>	$AP_{75}$	$AP_s$	$AP_m$	$AP_l$
FR [21]	5.6	12.3	4.6	-	-	-
Meta [57]	8.7	19.1	6.6	-	-	-
Fan <i>et al</i> . [10]	11.1	20.4	10.6	2.8	12.3	20.7
Fan et al. +INSTA	12.5	23.6	12.1	3.3	13.2	21.4

Table 5. The few-shot detection results of 6 different average precision (AP) on the test set, including MS COCO and PASCAL VOC datasets with 20-way 10-shot setting.

### 4.4. Ablation Study

In the following section, we conduct ablation studies to discuss and verify the effect of each component of our framework, including the instance-kernel, task-specific kernel, MSA *vs.* GAP, and we also evaluate some variants of the proposed INSTA to justify the selection of our current framework. In this study, we use the ProtoNet as the baseline, and the ResNet-12 is adopted as its backbone. Addi-

tionally, this study is conducted on the *mini*-ImageNet under the 5-way 5-shot setting. The results in Table 6 and Fig. 5 are used for analysis.

ID	Model	5-way 5-shot
(i)	ProtoNet	$79.46 \pm 0.48$
(ii)	ProtoNet w/ $oldsymbol{G}^{ta}$ w/o $\dot{oldsymbol{Q}}_i$	$81.56 \pm 0.57$
(iii)	ProtoNet w/ $oldsymbol{G}^{in}$ w/o $\dot{oldsymbol{Q}}_i$	$80.81 \pm 0.60$
(iv)	INSTA-ProtoNet w/o $\dot{m{Q}}_i$	$81.74 \pm 0.56$
(v)	INSTA-ProtoNet w/o $oldsymbol{G}^{in}$	$82.51 \pm 0.58$
(vi)	INSTA-ProtoNet w/o MSA	$82.07 \pm 0.56$
(vii)	INSTA-ProtoNet w/ $G_{m{Q}_i}^{in}$	$82.24 \pm 0.56$
(viii)	INSTA-ProtoNet w/o sharing weights	$81.36 \pm 0.59$
(ix)	INSTA-ProtoNet	$83.13 \pm 0.56$

Table 6. The ablation study of each component in our framework.

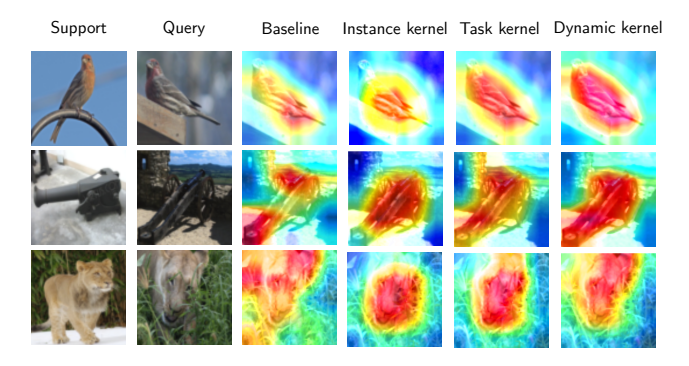


Figure 5. The heatmaps of different variants on top of ProtoNet as the baseline. Each column (from column 3-6) corresponds to a setting in Table 6. Baseline: (i), Instance kernel: (iii), Task kernel: (v), Dynamic kernel: (ix).

**Effectiveness of Task-Specific Kernel.** We study the effect of the task-specific kernel in this experiment (*i.e.*, (ii) in Table 6), where we only apply the task-specific kernel to support samples and leave the query unchanged. By comparing (i) and (ii), we can observe that our task-specific kernel improves the performance of ProtoNet by 2.10%. Moreover, we apply the task-specific kernel on the query in setting (v) (see the 5-th column in Fig. 5 for visualization), and we can observe a further improvement over the setting (ii), which verifies the effectiveness of our task-specific kernel.

**Effectiveness of Instance Kernel.** In setting (iii), we enable the instance kernel based on ProtoNet (*i.e.*, (i)) and the performance of ProtoNet is improved by 1.35% (see the 3-rd and 4-th columns in Fig. 5 for visualizations). Moreover, comparing setting (ii), where the only task-specific kernel is enabled, to setting (iv), where both task-specific and instance kernels are enabled, a performance improvement can also be observed. Both cases illustrate the effectiveness of our instance kernel.

Effectiveness of query adaptation. The purpose of this ex-

periment is to study the effect of the adaptation on the query feature. In setting (v), we enable the task-specific kernel on both support and query features but disable the instance kernel. Compared to setting (ii), where the task-specific kernel is enabled only on the support features, setting (v) yields a better performance. Furthermore, the comparison between setting (iv) and (ix) (see the 6-th column in Fig. 5) highlights the importance of adapting the query feature map using the task information for FSL tasks.

**Effectiveness of MSA.** In this study, we show the performance gap between using GAP and MSA (§ 3.3.1). In setting (vi) we replace the MSA in our final design (ix) with GAP. As the results in Table 6 showed, the MSA indeed helps with learning a more informative and representative dynamic kernel than GAP.

Instance Kernel for Query. In our framework, we only use task-specific kernels on the query feature map since the instance kernels obtained from support samples might not be instance level representative for the query sample but provide useful task information. Therefore, we perform extra experiments to verify whether the instance kernel obtained from the query itself can extract better features. As the result in (vii) indicates, the instance kernel extracted from the query feature map does not improve the performance, as compared to our final design.

Shared Dynamic Kernel Generator. We hypothesize that sharing the Dynamic Kernel Network for the task-specific kernel and instance kernel encourages learning a more representative instance kernel. To verify this, we further conduct an experiment where two independent dynamic kernel generators are used to produce the task-specific kernel and instance kernel. As the comparison between (ix) and (viii) shows, inferring the instance and task kernels using a shared weight dynamic kernel generator is an essential design choice.

### 5. Conclusion and Remark

In this paper, we propose to learn a dynamic embedding function realized by a novel dynamic kernel, which extracts features at both instance-level and task-level while encoding important frequency patterns. Our method improves the performance of several FSL models. This is demonstrated on 4 public few-shot classification datasets, including *mini*-ImageNet, *tiered*-ImageNet, CUB, and FC100 and a few-shot detection dataset, namely MS COO-PASCAL-VOC. We note that our context learning module aggregates all the support features; as such the required memory increases with the size of the support set during backpropagation. Additionally, we note that the we use the subset of the ImageNet (*mini*-ImageNet and *tiered*-ImageNet) which is known biased in terms of the gender and ethnicity.

## 6. Supplementary Material

In this supplementary material, we provide the implementation details of our model for few-shot classification and detection tasks. Furthermore, we provide extra experiments to verify the effectiveness of our proposed model. Finally, we provide further discussion of the MSA module.

### 6.1. Implementation Details

We first introduce the implementation, including the network, optimizer, training strategy and architecture for the few-shot classification task followed by that of few-shot detection task.

#### **6.1.1** Few-Shot Classification

Network and Optimizer. We use the ResNet-10 backbone [6] for the MAML and the ResNet-12 backbone [58. 59] for the other two baselines across all four benchmarks. Noted additional ResNet-18 backbone [62] is employed for the ProtoNet experiments on CUB. We fix the size of input images to 84 × 84 for ProtoNet and DeepEMD baselines and  $224 \times 224$  for MAML baseline. We use SGD optimizer for ProtoNet and DeepEMD experiments [58,59] and AdamW optimizer for MAML experiments [6] across all the datasets. For ProtoNet and DeepEMD baselines, we use L2 regularizer with 0.0005 weight decay factor. In the MAML baseline, the weight dacay factor is 0.01. For ResNet-18 and ResNet-10 backbones, we disable the average pooling and remove the last fully connected (FC) layer to produce the feature maps with size of  $512 \times 11 \times 11$  and  $512 \times 7 \times 7$ , respectively. In the ResNet-12 backbone, the network produces the feature map with a size of  $640 \times 5 \times 5$ . **Training.** We follow the good practice in the state-of-theart models [42, 58, 59], where the network training is split into two stages, i.e. pre-training and meta-training stages. During pre-training stage, the backbone network with a FC layer is trained on all the training classes of the dataset with the standard classification task. We select the network with the highest validation accuracy as the pre-trained backbone network for the meta-training stage. During metatraining stage, we follow the standard episodic training protocol [49] to train the entire model. We set a small learning rate (0.0002) for the backbone and a larger learning rate  $(0.0002 \times 25)$  for our modules during meta-training stage. Additionally, we use cosine annealing learning rate scheduler over 200 epochs. Finally, during meta-testing phase, an embedding optimization process is employed for our ProtoNet experiments, where we use the support samples to optimize the prototypes.

**Architecture.** The architecture of the dynamic kernel generator can be summarized into Table 7 (channel kernel network) and Table 8 (spatial kernel network). Furthermore,

we provide the architecture of the context learning module in Table 9.

layer name	output size	operation parameter
DCT	$1 \times 1$	640
conv1	$1 \times 1$	$1 \times 1$ , 128, stride 1
relu	$1 \times 1$	-
conv2	$1 \times 1$	$1 \times 1$ , 5760, stride 1
reshape	$3 \times 3$	640
sigmoid	$3 \times 3$	640
batch norm	$3 \times 3$	640

Table 7. The architecture of channel kernel network.

layer name	output size	operation parameter
conv1	$5 \times 5$	$1 \times 1$ , 9, stride 1
reshape	$3 \times 3$	25
batch norm	$3 \times 3$	25

Table 8. The architecture of spatial kernel network.

layer name	output size	operation parameter
conv1	$5 \times 5$	$1 \times 1$ , 1280, stride 1
batch norm	$5 \times 5$	1280
relu	$5 \times 5$	1280
conv2	$5 \times 5$	$1 \times 1$ , 1280, stride 1
batch norm	$5 \times 5$	1280
relu	$5 \times 5$	1280
summation	$5 \times 5$	-
conv3	$5 \times 5$	$1 \times 1$ , 1280, stride 1
batch norm	$5 \times 5$	1280
relu	$5 \times 5$	1280
conv4	$5 \times 5$	$1 \times 1$ , 640, stride 1
batch norm	$5 \times 5$	640
relu	$5 \times 5$	640

Table 9. The architecture of the context learning module.

### **6.1.2** Few-Shot Detection

For the few-shot detection task, we consider the method proposed by Fan *et al.* [10] as our baseline model, which inherits from the faster-R-CNN [37] framework. Similar to the few-shot classification task, we implement our method to produce dynamic kernels and perform convolution on the feature maps extracted by the backbone network (*i.e.* ResNet-50), which is followed by a region proposal network (RPN), a region of interest pooling (ROI pooling) operation, and the classification and bounding box regression heads, outputting the categories and bounding boxes for the objects to the query image. Notably, For a fair comparison,

we do not use any additional data augmentation. Please refer to [10] for more details of the framework and training strategy.

### 6.2. Additional Experiment Results

#### **6.2.1** Benchmark Results

In this part, we provide extra comparison between our model and other state-of-the-art models on *mini*-ImageNet and *tiered*-ImageNet in Table 10 and Table 11. We follow the evaluation protocol in our baseline implementations [6, 59], where 600 episodes are randomly sampled for both 1-shot and 5-shot settings in MAML experiment; 10,000 and 600 episodes are randomly sampled for 1-shot and 5-shot settings in ProtoNet and EMD experiments.

Model	Backbone	5-way 1-shot	5-way 5-shot
MetaOptNet [24]	ResNet-12	$62.64 \pm 0.61$	$78.63 \pm 0.46$
MetaOptNet-SVM [24]	ResNet-12	$64.09 \pm 0.62$	$80.00 \pm 0.45$
Neg-Margin [27]	ResNet-12	$63.85 \pm 0.81$	$81.57 \pm 0.56$
TADAM [33]	ResNet-12	$58.50 \pm 0.30$	$76.70 \pm 0.30$
TPN [29]	ResNet-12	59.46	75.65
DSN-MR [42]	ResNet-12	$64.60 \pm 0.72$	$79.51 \pm 0.50$
$E^{3}BM [30]$	ResNet-12	$63.80 \pm 0.40$	$80.10 \pm 0.30$
FEAT [58]	ResNet-12	$66.78 \pm 0.20$	$82.05 \pm 0.14$
CAN [17]	ResNet-12	$63.85 \pm 0.48$	$79.44 \pm 0.34$
ConstellationNet [56]	ResNet-12	$64.89 \pm 0.23$	$79.95 \pm 0.37$
FRN [54]	ResNet-12	$66.45 \pm 0.19$	$82.83 \pm 0.13$
InfoPatch [28]	ResNet-12	$67.67 \pm 0.45$	$82.44 \pm 0.31$
GLoFA [31]	ResNet-12	$66.12 \pm 0.42$	$81.37 \pm 0.33$
MELR [12]	ResNet-12	$67.40 \pm 0.43$	$83.40 \pm 0.28$
CNL [60]	ResNet-12	$67.96 \pm 0.98$	$83.36 \pm 0.51$
DMF [55]	ResNet-12	$67.76 \pm 0.46$	$82.71 \pm 0.31$
MAML* [13]	ResNet-10	$54.73 \pm 0.87$	$66.72 \pm 0.81$
INSTA-MAML*	ResNet-10	$56.41 \pm 0.87$	$71.56 \pm 0.75$
ProtoNet* [44]	ResNet-12	$62.29 \pm 0.33$	$79.46 \pm 0.48$
INSTA-ProtoNet*	ResNet-12	$67.01 \pm 0.30$	$83.13 \pm 0.56$
DeepEMD*♣ [59]	ResNet-12	$67.37 \pm 0.45$	$83.17 \pm 0.75$
INSTA-DeepEMD*♣	ResNet-12	$68.46 \pm 0.48$	$84.21 \pm 0.82$

Table 10. Few-shot classification accuracy and 95% confidence interval on *mini*-ImageNet with ResNet backbones.

### 6.2.2 Ablation Study

In this part, we provide extra ablation studies on the effect of the residual connection and the spatial size of our dynamic kernel.

**Residual Connection**. In this experiment, we study the effect of the residual connection in our framework. In setting (i) of the Table 12, we disable the residual connection between the adapted and original features. The result suggests that the residual connection is an essential design choice for our framework.

**Kernel Size.** We provide an extra study on the effect of the spatial size of our dynamic kernel. Given that the feature map extracted by ResNet-12 has spatial size  $5 \times 5$ , the dynamic kernel size is constrained smaller or equal to  $5 \times 5$ . Therefore, in this study, we compare the results

Model	Backbone	5-way 1-shot	5-way 5-shot
MetaOptNet [24]	ResNet-12	$68.23 \pm 0.23$	$84.03 \pm 0.56$
DSM-MR [42]	ResNet-12	$67.39 \pm 0.82$	$82.82 \pm 0.56$
$E^{3}BM [30]$	ResNet-12	$71.20 \pm 0.40$	$85.30 \pm 0.30$
FEAT [58]	ResNet-12	$70.80 \pm 0.23$	$84.79 \pm 0.16$
CAN [17]	ResNet-12	$69.89 \pm 0.51$	$84.23 \pm 0.37$
CNL [60]	ResNet-12	$73.42 \pm 0.95$	$87.72 \pm 0.75$
FRN [54]	ResNet-12	$72.06 \pm 0.22$	$86.89 \pm 0.14$
MELR [12]	ResNet-12	$72.14 \pm 0.51$	$87.01 \pm 0.35$
GLoFA [31]	ResNet-12	$69.75 \pm 0.33$	$83.58 \pm 0.42$
DMF [55]	ResNet-12	$71.89 \pm 0.52$	$85.96 \pm 0.35$
MAML* [13]	ResNet-10	$59.85 \pm 0.97$	$73.20 \pm 0.81$
INSTA-MAML*	ResNet-10	$63.34 \pm 0.92$	$78.01 \pm 0.71$
ProtoNet* [44]	ResNet-12	$68.25 \pm 0.23$	$84.01 \pm 0.56$
INSTA-ProtoNet*	ResNet-12	$70.65 \pm 0.33$	$85.76 \pm 0.59$
DeepEMD*♣ [59]	ResNet-12	$73.19 \pm 0.32$	$86.79 \pm 0.61$
INSTA-DeepEMD*♣	ResNet-12	$73.87 \pm 0.31$	$88.02 \pm 0.61$

Table 11. Few-shot classification accuracy and 95% confidence interval on *tiered*-ImageNet with ResNet backbones.

when the dynamic kernel size  $k = 5 \times 5$  to our final design  $(k = 3 \times 3)$ .

ID	Model	5-way 5-shot
(i)	INSTA-ProtoNet w/o residual	80.03
(ii)	INSTA-ProtoNet w/ $5 \times 5$ $G^{dy}$	82.43
(iii)	INSTA-ProtoNet	83.13

Table 12. The extra ablation study for the effect of the residual connection and spatial size of our dynamic kernel.

### 6.3. Multi-Spectral Attention

In this section, we provide more details for using the 2D-DCT to obtain the frequency-encoded vector. We first introduce the basis function of the 2D-DCT. The basis  $B_{u,v}^{a,b}$  of the 2D-DCT is given by:

$$B_{u,v}^{a,b} = \cos(\frac{\pi u}{h}(a+\frac{1}{2}))\cos(\frac{\pi v}{w}(b+\frac{1}{2})),\tag{7}$$

where u,v are the frequency components of a basis. Then the frequency-encoded vector of a 3D-tensor  $S^i \in \mathbb{R}^{\frac{c}{n} \times h \times w}$  can be obtained by:

$$m{ au}^i = \sum_{a=0}^{h-1} \sum_{b=0}^{w-1} m{S}_{:,a,b} B^{a,b}_{u_i,v_i}$$

s.t. 
$$i \in \{0, 1, \dots, n-1\},\$$

where  $\tau^i \in \mathbb{R}^{\frac{c}{n}}$  is the frequency-encoded vector, h and w are the height and width of the input signal. We pick the lowest 16 frequency components for our basis function according to [34]. Finally, we concatenate all the frequency-encoded vectors as:

$$\tau = \operatorname{concat}(\tau^0, \tau^1, \dots, \tau^{n-1}),$$
 (8)

where  $\boldsymbol{\tau} \in \mathbb{R}^c$ .

### References

- [1] Marcin Andrychowicz, Misha Denil, Sergio Gomez, Matthew W Hoffman, David Pfau, Tom Schaul, Brendan Shillingford, and Nando De Freitas. Learning to learn by gradient descent by gradient descent. In Advances in neural information processing systems, pages 3981–3989, 2016. 2
- [2] Antreas Antoniou, Harrison Edwards, and Amos Storkey. How to train your maml. In *International Conference on Learning Representations*, 2019.
- [3] Luca Bertinetto, Joao F Henriques, Philip Torr, and Andrea Vedaldi. Meta-learning with differentiable closed-form solvers. In *International Conference on Learning Representations*, 2018. 2
- [4] Luca Bertinetto, João F Henriques, Jack Valmadre, Philip HS Torr, and Andrea Vedaldi. Learning feed-forward one-shot learners. In *Proceedings of the 30th International Conference on Neural Information Processing Systems*, pages 523– 531, 2016. 2
- [5] Tolga Bolukbasi, Joseph Wang, Ofer Dekel, and Venkatesh Saligrama. Adaptive neural networks for efficient inference. In *International Conference on Machine Learning*, pages 527–536. PMLR, 2017. 2
- [6] Wei-Yu Chen, Yen-Cheng Liu, Zsolt Kira, Yu-Chiang Frank Wang, and Jia-Bin Huang. A closer look at few-shot classification. arXiv preprint arXiv:1904.04232, 2019. 2, 6, 7, 9, 10
- [7] Yinpeng Chen, Xiyang Dai, Mengchen Liu, Dongdong Chen, Lu Yuan, and Zicheng Liu. Dynamic convolution: Attention over convolution kernels. In *Proceedings of the IEEE/CVF Conference on Computer Vision and Pattern Recognition*, pages 11030–11039, 2020. 2, 4
- [8] Jonghyun Choi, Jayant Krishnamurthy, Aniruddha Kembhavi, and Ali Farhadi. Structured set matching networks for one-shot part labeling. In *Proceedings of the IEEE Conference on Computer Vision and Pattern Recognition*, pages 3627–3636, 2018.
- [9] Jia Deng, Wei Dong, Richard Socher, Li-Jia Li, Kai Li, and Li Fei-Fei. Imagenet: A large-scale hierarchical image database. In 2009 IEEE conference on computer vision and pattern recognition, pages 248–255. Ieee, 2009. 6
- [10] Qi Fan, Wei Zhuo, Chi-Keung Tang, and Yu-Wing Tai. Few-shot object detection with attention-rpn and multi-relation detector. In *Proceedings of the IEEE/CVF Conference on Computer Vision and Pattern Recognition*, pages 4013–4022, 2020. 5, 6, 7, 9, 10
- [11] Pengfei Fang, Mehrtash Harandi, and Lars Petersson. Kernel methods in hyperbolic spaces. In *Proceedings of the IEEE/CVF International Conference on Computer Vision*, pages 10665–10674, 2021. 2
- [12] Nanyi Fei, Zhiwu Lu, Tao Xiang, and Songfang Huang. Melr: Meta-learning via modeling episode-level relationships for few-shot learning. In *International Conference on Learning Representations*, 2020. 2, 10
- [13] Chelsea Finn, Pieter Abbeel, and Sergey Levine. Model-agnostic meta-learning for fast adaptation of deep networks. *arXiv preprint arXiv:1703.03400*, 2017. 1, 2, 5, 6, 7, 10

- [14] Sebastian Flennerhag, Andrei A Rusu, Razvan Pascanu, Francesco Visin, Hujun Yin, and Raia Hadsell. Metalearning with warped gradient descent. arXiv preprint arXiv:1909.00025, 2019.
- [15] Luca Franceschi, Paolo Frasconi, Saverio Salzo, Riccardo Grazzi, and Massimilano Pontil. Bilevel programming for hyperparameter optimization and meta-learning. arXiv preprint arXiv:1806.04910, 2018. 2
- [16] David Ha, Andrew Dai, and Quoc V Le. Hypernetworks. arXiv preprint arXiv:1609.09106, 2016. 2
- [17] Ruibing Hou, Hong Chang, Bingpeng Ma, Shiguang Shan, and Xilin Chen. Cross attention network for few-shot classification. arXiv preprint arXiv:1910.07677, 2019. 2, 6, 7, 10
- [18] Jie Hu, Li Shen, and Gang Sun. Squeeze-and-excitation networks. In *Proceedings of the IEEE conference on computer* vision and pattern recognition, pages 7132–7141, 2018. 4
- [19] Gao Huang, Danlu Chen, Tianhong Li, Felix Wu, Laurens van der Maaten, and Kilian Weinberger. Multi-scale dense networks for resource efficient image classification. In *International Conference on Learning Representations*, 2018.
- [20] Xu Jia, Bert De Brabandere, Tinne Tuytelaars, and Luc V Gool. Dynamic filter networks. Advances in neural information processing systems, 29:667–675, 2016.
- [21] Bingyi Kang, Zhuang Liu, Xin Wang, Fisher Yu, Jiashi Feng, and Trevor Darrell. Few-shot object detection via feature reweighting. In *Proceedings of the IEEE/CVF International Conference on Computer Vision*, pages 8420–8429, 2019. 7
- [22] Gregory Koch, Richard Zemel, Ruslan Salakhutdinov, et al. Siamese neural networks for one-shot image recognition. In *ICML deep learning workshop*, volume 2. Lille, 2015. 2
- [23] Alex Krizhevsky, Geoffrey Hinton, et al. Learning multiple layers of features from tiny images. 2009. 6
- [24] Kwonjoon Lee, Subhransu Maji, Avinash Ravichandran, and Stefano Soatto. Meta-learning with differentiable convex optimization. In *Proceedings of the IEEE Conference on Computer Vision and Pattern Recognition*, pages 10657–10665, 2019. 2, 6, 7, 10
- [25] Yoonho Lee and Seungjin Choi. Gradient-based metalearning with learned layerwise metric and subspace. In *International Conference on Machine Learning*, pages 2927–2936. PMLR, 2018. 2
- [26] Hongyang Li, David Eigen, Samuel Dodge, Matthew Zeiler, and Xiaogang Wang. Finding task-relevant features for fewshot learning by category traversal. In *Proceedings of the IEEE Conference on Computer Vision and Pattern Recogni*tion, pages 1–10, 2019. 2
- [27] Bin Liu, Yue Cao, Yutong Lin, Qi Li, Zheng Zhang, Mingsheng Long, and Han Hu. Negative margin matters: Understanding margin in few-shot classification. *arXiv preprint arXiv:2003.12060*, 2020. 6, 7, 10
- [28] Chen Liu, Yanwei Fu, Chengming Xu, Siqian Yang, Jilin Li, Chengjie Wang, and Li Zhang. Learning a few-shot embedding model with contrastive learning. In *Proceedings of the AAAI Conference on Artificial Intelligence*, volume 35, pages 8635–8643, 2021. 2, 6, 10

- [29] Yanbin Liu, Juho Lee, Minseop Park, Saehoon Kim, Eunho Yang, Sung Ju Hwang, and Yi Yang. Learning to propagate labels: Transductive propagation network for few-shot learning. *arXiv preprint arXiv:1805.10002*, 2018. 2, 10
- [30] Yaoyao Liu, Bernt Schiele, and Qianru Sun. An ensemble of epoch-wise empirical bayes for few-shot learning. In *European Conference on Computer Vision*, pages 404–421. Springer, 2020. 2, 10
- [31] Su Lu, Han-Jia Ye, and De-Chuan Zhan. Tailoring embedding function to heterogeneous few-shot tasks by global and local feature adaptors. In *Proceedings of the AAAI Conference on Artificial Intelligence*, volume 35, pages 8776–8783, 2021. 1, 2, 6, 7, 10
- [32] Alex Nichol, Joshua Achiam, and John Schulman. On first-order meta-learning algorithms. *arXiv preprint arXiv:1803.02999*, 2018. 1, 2
- [33] Boris N Oreshkin, Pau Rodriguez, and Alexandre Lacoste. Tadam: task dependent adaptive metric for improved fewshot learning. In *Proceedings of the 32nd International Conference on Neural Information Processing Systems*, pages 719–729, 2018. 2, 5, 6, 7, 10
- [34] Zequn Qin, Pengyi Zhang, Fei Wu, and Xi Li. Fcanet: Frequency channel attention networks. arXiv preprint arXiv:2012.11879, 2020. 4, 10
- [35] Sachin Ravi and H. Larochelle. Optimization as a model for few-shot learning. In *ICLR*, 2017. 6
- [36] Mengye Ren, Eleni Triantafillou, Sachin Ravi, Jake Snell, Kevin Swersky, Joshua B Tenenbaum, Hugo Larochelle, and Richard S Zemel. Meta-learning for semi-supervised fewshot classification. arXiv preprint arXiv:1803.00676, 2018.
  1. 6
- [37] Shaoqing Ren, Kaiming He, Ross Girshick, and Jian Sun. Faster r-cnn: Towards real-time object detection with region proposal networks. Advances in neural information processing systems, 28:91–99, 2015.
- [38] Andrei A Rusu, Dushyant Rao, Jakub Sygnowski, Oriol Vinyals, Razvan Pascanu, Simon Osindero, and Raia Hadsell. Meta-learning with latent embedding optimization. arXiv preprint arXiv:1807.05960, 2018. 2
- [39] Victor Garcia Satorras and Joan Bruna Estrach. Few-shot learning with graph neural networks. In *International Conference on Learning Representations*, 2018. 2
- [40] Zhiqiang Shen, Zechun Liu, Jie Qin, Marios Savvides, and Kwang-Ting Cheng. Partial is better than all: Revisiting finetuning strategy for few-shot learning. In *Proceedings of the AAAI Conference on Artificial Intelligence*, volume 35, pages 9594–9602, 2021. 7
- [41] Pranav Shyam, Shubham Gupta, and Ambedkar Dukkipati. Attentive recurrent comparators. In *International Conference on Machine Learning*, pages 3173–3181. PMLR, 2017.
- [42] Christian Simon, Piotr Koniusz, Richard Nock, and Mehrtash Harandi. Adaptive subspaces for few-shot learning. In Proceedings of the IEEE/CVF Conference on Computer Vision and Pattern Recognition, pages 4136–4145, 2020. 2, 9, 10

- [43] Christian Simon, Piotr Koniusz, Richard Nock, and Mehrtash Harandi. On modulating the gradient for metalearning. In *European Conference on Computer Vision*, pages 556–572. Springer, 2020. 2
- [44] Jake Snell, Kevin Swersky, and Richard Zemel. Prototypical networks for few-shot learning. In *Advances in neural information processing systems*, pages 4077–4087, 2017. 1, 2, 5, 6, 7, 10
- [45] Flood Sung, Yongxin Yang, Li Zhang, Tao Xiang, Philip HS Torr, and Timothy M Hospedales. Learning to compare: Relation network for few-shot learning. In *Proceedings of the IEEE Conference on Computer Vision and Pattern Recogni*tion, pages 1199–1208, 2018. 1, 2, 7
- [46] Surat Teerapittayanon, Bradley McDanel, and Hsiang-Tsung Kung. Branchynet: Fast inference via early exiting from deep neural networks. In 2016 23rd International Conference on Pattern Recognition (ICPR), pages 2464–2469. IEEE, 2016. 2
- [47] Eleni Triantafillou, Richard Zemel, and Raquel Urtasun. Few-shot learning through an information retrieval lens. In Proceedings of the 31st International Conference on Neural Information Processing Systems, pages 2252–2262, 2017.
- [48] Andreas Veit and Serge Belongie. Convolutional networks with adaptive inference graphs. In *Proceedings of the Euro*pean Conference on Computer Vision (ECCV), pages 3–18, 2018. 2
- [49] Oriol Vinyals, Charles Blundell, Timothy Lillicrap, Daan Wierstra, et al. Matching networks for one shot learning. In Advances in neural information processing systems, pages 3630–3638, 2016. 1, 2, 9
- [50] Catherine Wah, Steve Branson, Peter Welinder, Pietro Perona, and Serge Belongie. The caltech-ucsd birds-200-2011 dataset. 2011. 6
- [51] Xin Wang, Fisher Yu, Zi-Yi Dou, Trevor Darrell, and Joseph E Gonzalez. Skipnet: Learning dynamic routing in convolutional networks. In *Proceedings of the European Conference on Computer Vision (ECCV)*, pages 409–424, 2018. 2
- [52] Yan Wang, Wei-Lun Chao, Kilian Q Weinberger, and Laurens van der Maaten. Simpleshot: Revisiting nearest-neighbor classification for few-shot learning. arXiv preprint arXiv:1911.04623, 2019.
- [53] Yaqing Wang, Quanming Yao, James T Kwok, and Lionel M Ni. Generalizing from a few examples: A survey on fewshot learning. ACM Computing Surveys (CSUR), 53(3):1–34, 2020. 1
- [54] Davis Wertheimer, Luming Tang, and Bharath Hariharan. Few-shot classification with feature map reconstruction networks. In *Proceedings of the IEEE/CVF Conference on Computer Vision and Pattern Recognition*, pages 8012–8021, 2021. 2, 6, 7, 10
- [55] Chengming Xu, Yanwei Fu, Chen Liu, Chengjie Wang, Jilin Li, Feiyue Huang, Li Zhang, and Xiangyang Xue. Learning dynamic alignment via meta-filter for few-shot learning. In Proceedings of the IEEE/CVF Conference on Computer Vision and Pattern Recognition, pages 5182–5191, 2021. 1, 2, 6, 7, 10

- [56] Weijian Xu, Huaijin Wang, Zhuowen Tu, et al. Attentional constellation nets for few-shot learning. In *International Conference on Learning Representations*, 2020. 2, 7, 10
- [57] Xiaopeng Yan, Ziliang Chen, Anni Xu, Xiaoxi Wang, Xiaodan Liang, and Liang Lin. Meta r-cnn: Towards general solver for instance-level low-shot learning. In *Proceedings of the IEEE/CVF International Conference on Computer Vision*, pages 9577–9586, 2019.
- [58] Han-Jia Ye, Hexiang Hu, De-Chuan Zhan, and Fei Sha. Few-shot learning via embedding adaptation with set-to-set functions. In *Proceedings of the IEEE/CVF Conference on Computer Vision and Pattern Recognition*, pages 8808–8817, 2020. 1, 2, 6, 7, 9, 10
- [59] Chi Zhang, Yujun Cai, Guosheng Lin, and Chunhua Shen. Deepemd: Few-shot image classification with differentiable earth mover's distance and structured classifiers. In *Proceedings of the IEEE/CVF Conference on Computer Vision and Pattern Recognition*, pages 12203–12213, 2020. 1, 2, 5, 6, 7, 9, 10
- [60] Jiabao Zhao, Yifan Yang, Xin Lin, Jing Yang, and Liang He. Looking wider for better adaptive representation in few-shot learning. In *Proceedings of the AAAI Conference on Artifi*cial Intelligence, volume 35, pages 10981–10989, 2021. 2, 10
- [61] Jingkai Zhou, Varun Jampani, Zhixiong Pi, Qiong Liu, and Ming-Hsuan Yang. Decoupled dynamic filter networks. In Proceedings of the IEEE/CVF Conference on Computer Vision and Pattern Recognition, pages 6647–6656, 2021. 1, 2, 3
- [62] Imtiaz Ziko, Jose Dolz, Eric Granger, and Ismail Ben Ayed. Laplacian regularized few-shot learning. In *Inter*national Conference on Machine Learning, pages 11660– 11670. PMLR, 2020. 9